



Search for $ZH \rightarrow \ell^+ \ell^- b\bar{b}$ production in 9.7 fb^{-1} of $p\bar{p}$ collisions

The DØ Collaboration
URL <http://www-d0.fnal.gov>

Dated March 5, 2012

We present a search for a standard model (SM) Higgs boson produced in association with a Z boson in 9.7 fb^{-1} of $p\bar{p}$ collisions, collected with the D0 detector at the Fermilab Tevatron at $\sqrt{s} = 1.96 \text{ TeV}$. Selected events contain one reconstructed $Z \rightarrow e^+e^-$ or $Z \rightarrow \mu^+\mu^-$ candidate and at least two jets, including at least one b -tagged jet. The data are consistent with the background expected from other SM processes. Upper limits at 95% C.L. on the ZH production cross section times branching ratio are set for Higgs boson masses $100 < M_H < 150 \text{ GeV}$. The observed (expected) limit for $M_H = 115 \text{ GeV}$ is a factor of 3.7 (4.2) larger than the SM prediction.

Preliminary Results for the Winter 2012 Conferences

I. INTRODUCTION

In the standard model (SM), the spontaneous breakdown of the electroweak gauge symmetry generates masses for the W and Z bosons and produces a residual massive particle, the Higgs boson, which has so far eluded detection. The discovery of the Higgs boson would be a remarkable addition to the list of experimentally confirmed SM predictions. The combination of constraints from direct searches at LEP [1] and from precision electroweak observables [2] result in a preferred range for the Higgs boson mass of $114.4 < M_H < 185$ GeV at 95% C.L. The regions of $156 < M_H < 177$ GeV and $100 < M_H < 108$ GeV are excluded by a combination of searches at CDF and DØ [3]. The most recent LHC results [4] extend the excluded regions to $127 < M_H < 600$ GeV. For Higgs boson masses $M_H \lesssim 135$ GeV, the primary decay is to $b\bar{b}$, which has copious background at the Tevatron collider. Consequently, sensitivity to a low-mass Higgs boson is predominantly from its production in association with a W or Z boson.

We present a search for $ZH \rightarrow \ell^+\ell^-b\bar{b}$, where ℓ is either a muon or an electron. The search for $ZH \rightarrow \nu\bar{\nu}b\bar{b}$ is treated elsewhere [5]. The data for this analysis were collected at the Fermilab Tevatron Collider by the D0 detector [6] from April 2002 to February 2006 (Run IIa), and from June 2006 to September 2011 (Run IIb). Between Run IIa and Run IIb, a new layer of the silicon microstrip tracker was installed, and the trigger system was upgraded [7]. The analyzed events were acquired predominantly with triggers that provide real-time identification of electron and muon candidates. However, events satisfying any trigger requirement are considered in this analysis.

This note documents an update to previous searches in the same final states [8–11]. We reanalyze all four lepton channels, ee , ee_{ICR} , $\mu\mu$ and $\mu\mu_{\text{trk}}$ (defined in Section III), using the full Run II dataset, corresponding to an integrated luminosity of 9.7 fb^{-1} after data quality requirements were invoked.

II. DØ DETECTOR

The D0 detector [6] comprises a central tracking system in a 1.9 T superconducting solenoidal magnet, surrounded by a central preshower (CPS) detector, a liquid-argon sampling calorimeter, and a muon system. The tracking system, a silicon microstrip tracker (SMT) and a scintillating fiber tracker (CFT), provides coverage for charged particles in the pseudorapidity range $|\eta| < 3$ [12]. The CPS is located immediately before the inner layer of the calorimeter, and has about one radiation length of absorber, followed by three layers of scintillating strips. The calorimeter consists of a central cryostat with coverage of $|\eta| < 1.1$, and two end cryostats covering up to $|\eta| \approx 4.2$. The muon system resides beyond the calorimeter and consists of a layer of tracking detectors and scintillation trigger counters before 1.8 T iron toroidal magnet, followed by two similar layers after the toroid. The muon system provides coverage to $|\eta| < 2$.

III. EVENT SELECTION

The event selection requires a primary $p\bar{p}$ interaction vertex (PV) that has at least three associated tracks, and is located within ± 60 cm of the center of the detector along the beam direction. Selected events must also contain a $Z \rightarrow \ell^+\ell^-$ candidate with a dilepton invariant mass $60 < m_{\ell\ell} < 150$ GeV.

The dimuon ($\mu\mu$) selection requires at least two muons identified in the muon system, matched to central tracks (referred to as combined muons) with transverse momenta $p_T > 10$ GeV. For each muon, we calculate the combined tracking and calorimeter isolation, and require that the product of the combined isolation for the two muons is smaller than a given value, such that one muon does not have to be isolated if the other muon is sufficiently well isolated. Each muon-associated track must satisfy $|\eta_{\text{det}}| < 2$, where η_{det} is the pseudorapidity measured with respect to the center of the detector. At least one muon must have $|\eta_{\text{det}}| < 1.5$ and $p_T > 15$ GeV. The distance of closest approach of each muon-associated track to the PV in the plane transverse to the beam direction, d_{PV} , must be less than 0.04 cm for tracks with at least one hit in the silicon microstrip tracker (SMT). A track without any SMT hits must have $d_{PV} < 0.2$ cm, and its p_T is corrected through a constraint to the position of the PV. To reduce contamination from cosmic rays, the muon-associated tracks must not be back-to-back in η and ϕ . The two muon-associated tracks must also have opposite charge.

The $\mu\mu_{\text{trk}}$ selection is designed to recover dimuon events in which one muon is not identified in the muon system. This selection requires exactly one combined muon with $|\eta_{\text{det}}| < 1.5$ and $p_T > 15$ GeV. To ensure that the $\mu\mu$ and $\mu\mu_{\text{trk}}$ selections do not overlap, events containing any additional combined muons with $|\eta_{\text{det}}| < 2$ and $p_T > 10$ GeV are rejected. In addition, a central track with $|\eta_{\text{det}}| < 2$ and $p_T > 20$ GeV must be present. This track-only muon is only reconstructed in the central tracking system, and is required to have at least one SMT hit and $d_{PV} < 0.02$ cm. It is also required to be isolated in both the tracker and the calorimeter. The combined muon and track-only muon must have opposite charges. For the very small fraction of events with more than one track passing these requirements, the track whose invariant mass with the combined muon is closest to the Z boson mass (91.2 GeV) is chosen.

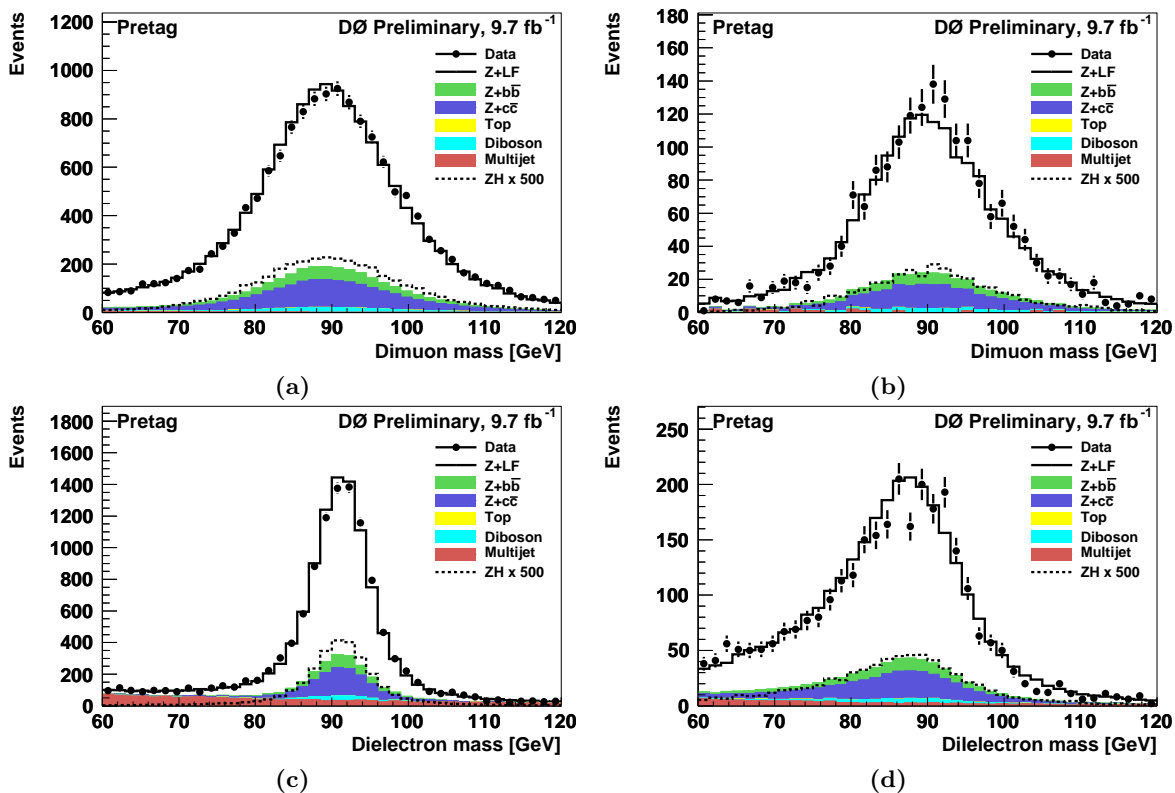


FIG. 1: The dilepton mass spectra in the (a) $\mu\mu$, (b) $\mu\mu_{\text{trk}}$, (c) ee and (d) ee_{ICR} channels. Distributions are shown in the “pretag” control sample, in which all selection requirements except b -tagging are applied. Signal distributions, for $M_H = 115$ GeV, are scaled by a factor of 500.

The dielectron (ee) selection requires at least two electrons with $p_T > 15$ GeV that pass selection requirements based on the energy deposition and shower shape in the calorimeter and the CPS. The two electrons are required to be isolated in both the tracker and the calorimeter. At least one electron must be identified in the central calorimeter (CC, $|\eta_{\text{det}}| < 1.1$), and a second electron either in the CC or end calorimeter (EC, $1.5 < |\eta_{\text{det}}| < 2.5$). The CC electrons must match central tracks or a set of hits in the tracker consistent with that of an electron trajectory.

The ee_{ICR} selection requires exactly one electron in either the CC or EC with $p_T > 15$ GeV, and an “ICR track” pointing toward one of the inter-cryostat regions (ICR) of the calorimeter, $1.1 < |\eta_{\text{det}}| < 1.5$, where the electromagnetic coverage is limited. The ICR track must be isolated and matched to a calorimeter energy deposit with $E_T > 15$ GeV. When the electron is found in the EC, the ICR electron candidate is required to be in the adjoining inter-cryostat region.

Jets are reconstructed in the calorimeter using the iterative midpoint cone algorithm [13] with a cone of radius 0.5 in the plane of rapidity and azimuth. The energy scale of jets is corrected for detector response, presence of noise and multiple interactions, and energy deposited outside of the reconstructed jet cone. At least two jets with $p_T > 20$ GeV and $|\eta_{\text{det}}| < 2.5$ are required. For the ee and ee_{ICR} selections, jets must be separated from an electron by $\Delta\mathcal{R} = \sqrt{\Delta\eta^2 + \Delta\phi^2} > 0.5$. In the $\mu\mu_{\text{trk}}$ selection, the isolated track must be separated by $\Delta\mathcal{R} > 0.5$ from all jets. To reduce the impact from multiple interactions at high instantaneous luminosities, jets must contain at least two associated tracks matched to the PV. To improve our background modeling, we also require the imbalance of transverse momentum in each event to be less than 50 GeV and that the separation in azimuth between the Z boson and the dijet system is at least 1.7 radians. The dimuon and dielectron mass spectra, after requiring two leptons and at least two jets are shown in Fig. 1. In this Figure, and others throughout this note, the ZH signal shown is for $M_H = 115$ GeV. The invariant mass of the dijet system (constructed from the two jets with the highest p_T) in the combination of all selections is shown in Fig 2. In this note, we use “inclusive” to denote the events selection with requiring two leptons, and use “pretag” for further requiring at least two jets.

To distinguish events containing a $H \rightarrow b\bar{b}$ decay from background processes involving light quarks and gluons, jets are identified as likely to contain b -quarks (b -tagged) if they pass “loose” or “tight” requirements on the output of a boosted decision tree trained to separate b -jets from light jets. This discriminant is an improved version of the neural

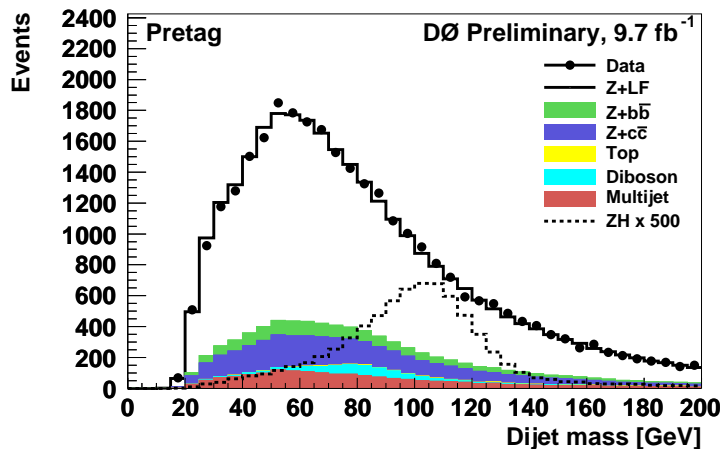


FIG. 2: Distribution of the dijet invariant mass in the combined ee , ee_{ICR} , $\mu\mu$ and $\mu\mu_{\text{trk}}$ sample after requiring two leptons and at least two jets (pretag). The signal distribution is scaled by a factor of 500.

net b -tagging discriminant described in Ref. [14]. For $|\eta| < 1.1$ and $p_T \approx 50$ GeV, the b -tagging efficiency for b -jets and the misidentification rate of light jets are, respectively, 72% and 6.7% for loose b -tags, and 47% and 0.4% for tight b -tags. Events with at least one tight and one loose b -tag are classified as double-tagged (DT). Events not in the DT sample that contain a single tight b -tag are classified as single-tagged (ST). The dijet $H \rightarrow b\bar{b}$ candidate is composed of the two highest p_T tagged jets in DT events, and the tagged jet plus the highest p_T non-tagged jet in ST events.

IV. BACKGROUND ESTIMATION

The dominant background process is the production of a Z boson in association with jets, with the Z decaying to dileptons (Z +jets). The light-flavor component (Z +LF) includes jets from only light quarks (uds) or gluons. The heavy-flavor component (Z +HF) includes non-resonant $Z + b\bar{b}$ which has the same final state as the signal, and non-resonant $Z + c\bar{c}$ production. The remaining backgrounds are from $t\bar{t}$ and diboson production, and from multijet events in which jets are misidentified as leptons. We simulate ZH and inclusive diboson production with PYTHIA [15]. In the ZH samples, we consider the $\ell^+\ell^-b\bar{b}$, $\ell^+\ell^-c\bar{c}$, and $\ell^+\ell^-\tau^+\tau^-$ final states. The Z +jets and $t\bar{t} \rightarrow \ell^+\nu b\ell^-\bar{\nu}b$ processes are simulated with ALPGEN [16]. All simulated samples are generated using the CTEQ6L1 [17] leading-order parton distribution function (PDF).

The events generated with ALPGEN use PYTHIA for parton showering and hadronization. Because this procedure can generate additional jets, we use a matching procedure to avoid double counting partons produced by ALPGEN and those subsequently added by the showering in PYTHIA. All samples are processed using a detector simulation program based on GEANT3 [18], and the same offline reconstruction algorithms used to process the data. Events from randomly chosen beam crossings are overlaid on the generated events to model the effect of multiple $p\bar{p}$ interactions and detector noise.

The cross section and branching ratio for signal are taken from Refs. [19, 20]. For the $t\bar{t}$ and diboson processes, the next-to-leading order (NLO) cross sections are used [21, 22]. The inclusive Z -boson cross section is scaled to next-to-NLO [23]. Additional NLO heavy-flavor corrections, calculated from MCFM, are applied to $Z + b\bar{b}$ and $Z + c\bar{c}$. To improve the modeling of the p_T distribution of the Z boson, the simulated Z boson events are reweighted to be consistent with the observed dielectron p_T spectrum in data [24].

The energies of simulated jets are modified to reproduce the resolution and energy scale observed in data. Scale factors are applied to account for differences in reconstruction efficiency between the data and simulation. Additional corrections are applied to improve agreement between data and background simulation, using two control samples with negligible signal contributions: an “inclusive” sample in which we apply only the lepton selection requirements; and a “pretag” sample that is obtained by applying all selection requirements except b -tagging. The $\mu\mu$, $\mu\mu_{\text{trk}}$ and ee_{ICR} distributions are corrected for trigger efficiencies. For the ee channel, no correction is applied as the combination of all triggers is nearly 100% efficient. To improve upon the ALPGEN modeling of Z +jets, motivated by a comparison with the SHERPA generator [25], events are reweighted so that the three kinematic distributions. These kinematic distributions are the pseudorapidities η of the two jets and the $\Delta\eta$ between them. In our signal samples, we correct the generator level p_T of the ZH system to match the distribution from RESBOS [26].

	Data	Total Background	Multijet	$Z+LF$	$Z+HF$	Other	ZH
inclusive	1 796 610	1 792 340	163 951	1 580 613	45 364	2412	24
pretag	31 376	31 322	1 833	23 463	5 324	702	15
ST	859	911	41	87	715	68	4.0
DT	300	320	10.2	5.7	245	59	4.3

TABLE I: Expected and observed event yields for all lepton channels combined after requiring two leptons (inclusive), after also requiring at least two jets (pretag), and after requiring exactly one (ST) or at least two (DT) b -tags. The “Other” column includes diboson and $t\bar{t}$ event yields. The ZH sample yields are for $M_H = 115$ GeV. Expected yields are obtained following the background normalization procedure described in Section IV

Channel	ee	ee_{ICR}	$\mu\mu$	$\mu\mu_{\text{trk}}$
ST	1.48	0.36	1.93	0.23
DT	1.60	0.40	2.08	0.24

TABLE II: Signal yields in the ST and DT samples for each channel, assuming $M_H = 115$ GeV.

The multijet backgrounds are estimated from control samples in the data. For the $\mu\mu$ channel, the multijet control sample consists of events that fail the muon isolation requirements, but otherwise pass the event selection. For the $\mu\mu_{\text{trk}}$ channel, the combined muon and track must have same-sign charge. For the ee channel, the electrons must fail isolation and shower shape requirements. For the ee_{ICR} channel, the electron in the ICR must fail a requirement on the shape of the electromagnetic shower in the calorimeter.

The normalizations of the multijet background and all simulated samples (both signal and background) are adjusted by scale factors determined from a simultaneous fit to the $m_{\ell\ell}$ distributions in the 0 jet, 1 jet and ≥ 2 jet samples of each lepton selection. This improves the accuracy of the background model and reduces the impact of systematic uncertainties that affect pretag event yields (e.g., uncertainties on luminosity and lepton identification). The region $40 < m_{\ell\ell} < 60$ GeV, where the multijet contribution is most prominent, is included in the fit to normalize the multijet control samples to the actual multijet contribution. The inclusive sample constrains the lepton trigger and identification efficiencies, while the pretag sample, which includes jet requirements, is used to correct the Z +jets cross section by a common scale factor $k_{Z+\text{jets}}$ (≈ 1). The total event yields after applying all corrections and normalization factors are shown in Table I. The ST and DT signal yields for the individual channels are displayed in Table II.

V. MULTIVARIATE ANALYSIS

To exploit the fully constrained kinematics of the $ZH \rightarrow \ell^+ \ell^- b\bar{b}$ process, the energies of the candidate leptons and jets are adjusted within their experimental resolutions with a likelihood fit that constrains $m_{\ell\ell}$ to the mass and width of the Z , and the p_T of the $\ell^+ \ell^- b\bar{b}$ system to the distribution expected for ZH events. The kinematic fit improves the dijet mass resolution by 10–15%. Distributions of the dijet invariant mass spectra and leading jet p_T distributions, before and after adjustment by the kinematic fit, are shown in Figs. 3 and 4.

A multivariate analysis combines the most significant kinematic information into a single discriminant. Well-modeled kinematic variables are chosen as inputs for the analysis: the transverse momenta of the two b -jet candidates and the dijet mass, before and after the jet energies are adjusted by the kinematic fit; angular differences within and between the dijet and dilepton systems; the opening angle between the proton beam and the Z candidate in the rest frame of the Z boson [27]; and composite kinematic variables, such as the p_T of the dijet system and the scalar sum of the p_T values of the leptons and jets. A complete list of input variables is shown in Table III, and some sample input distributions are shown in Fig. 5. For each assumed value of M_H a separate random forest (RF), consisting of 500 decision trees [28], is trained separately for ST and DT events. Each tree uses a randomly chosen subset of the simulated signal and background events. At each decision of each tree, a subset of nine of the inputs is randomly chosen for consideration. The RF output is the average of the output from each decision tree. The RF outputs for the ee , ee_{ICR} , $\mu\mu$ and $\mu\mu_{\text{trk}}$ channels combined are shown separately for pretag, ST and DT events in Figs. 6 and 7.

VI. SYSTEMATIC UNCERTAINTIES

Systematic uncertainties resulting from the background normalization are assessed for the multijet contribution (1–70%, depending on the channel) and from uncertainties on lepton efficiency effects (4%). The normalization of

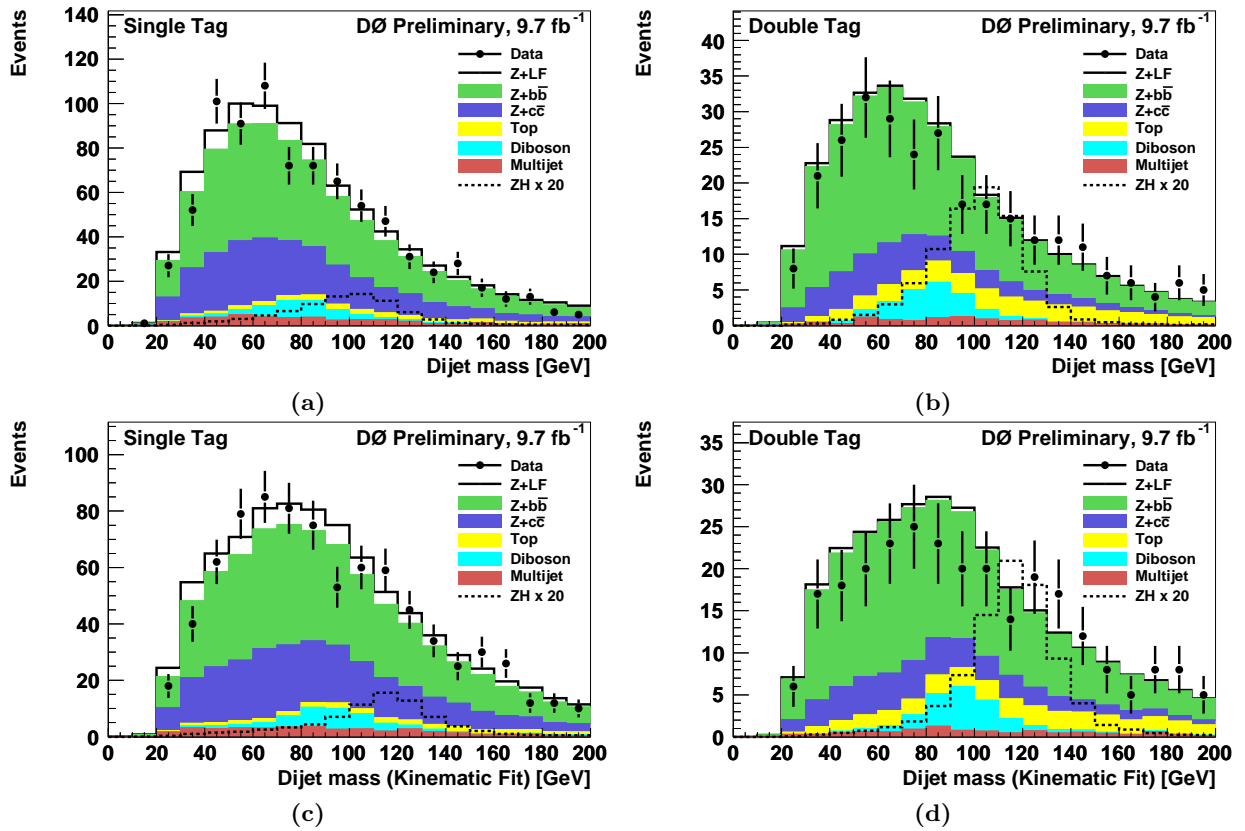


FIG. 3: Dijet invariant mass distributions before the kinematic fit in (a) ST events, and (b) DT events; and after the kinematic fit in (c) ST events and (d) DT events, combined for all lepton channels. Signal ($M_H = 115$ GeV) distributions are shown with the SM cross section multiplied by 20.

variables	definition
$m_{bb}(m_{bb}^{fit})$	invariant mass of the dijet system before (after) kinematic fit
p_T^{bb}	transverse momentum of the dijet system before kinematic fit
$p_T^{b1}(p_T^{b1,fit})$	transverse momentum of the leading jet before (after) kinematic fit
$p_T^{b2}(p_T^{b2,fit})$	transverse momentum of the other jet before (after) kinematic fit
$\Delta\phi(b_1, b_2)$	$\Delta\phi$ between the two jets in the dijet system
$\Delta\eta(b_1, b_2)$	$\Delta\eta$ between the two jets in the dijet system
$m(\sum \vec{j}_i)$	invariant mass of all jets in the event (the multijet mass)
$p_T(\sum \vec{j}_i)$	transverse momentum of all jets in the event
p_T^Z	transverse momentum of the dilepton system
$\Delta\eta(\ell_1, \ell_2)$	$\Delta\eta$ between the two leptons
$\Delta\phi(\ell_1, \ell_2)$	$\Delta\phi$ between the two leptons
$\text{colinearity}(\ell_1, \ell_2)$	cosine of the angle between the two leptons (colinearity)
$\Delta\phi(Z, bb)$	angle between the dilepton and dijet system
$\cos\theta^*$	angle between the incoming proton and the Z in the zero momentum frame [27]
$m(\ell\ell bb)$	Invariant mass of the dilepton plus dijet system
$H_T(\ell\ell bb)$	Scalar sum of the transverse momenta of the leptons and the 2 jets assigned to the H decay

TABLE III: Variables used for the RF training.

the Z +jets sample to match the pretag data constrains that sample to the statistical uncertainty of the pretag data ($<1\%$). However, the normalizations of the $t\bar{t}$, diboson, and ZH samples are sensitive to the ratios of these processes' cross sections to the Z cross section, for which we assign an uncertainty of 6%. The normalization to the pretag data, which is dominated by Z +LF, does not strongly constrain the cross sections of other processes. For Z +HF, a cross section uncertainty of 20% is determined from Ref. [21]. For other backgrounds, the uncertainties are 6%–10%. For the signal, the cross section uncertainty is 6% [19]. The normalization procedure described in Section IV

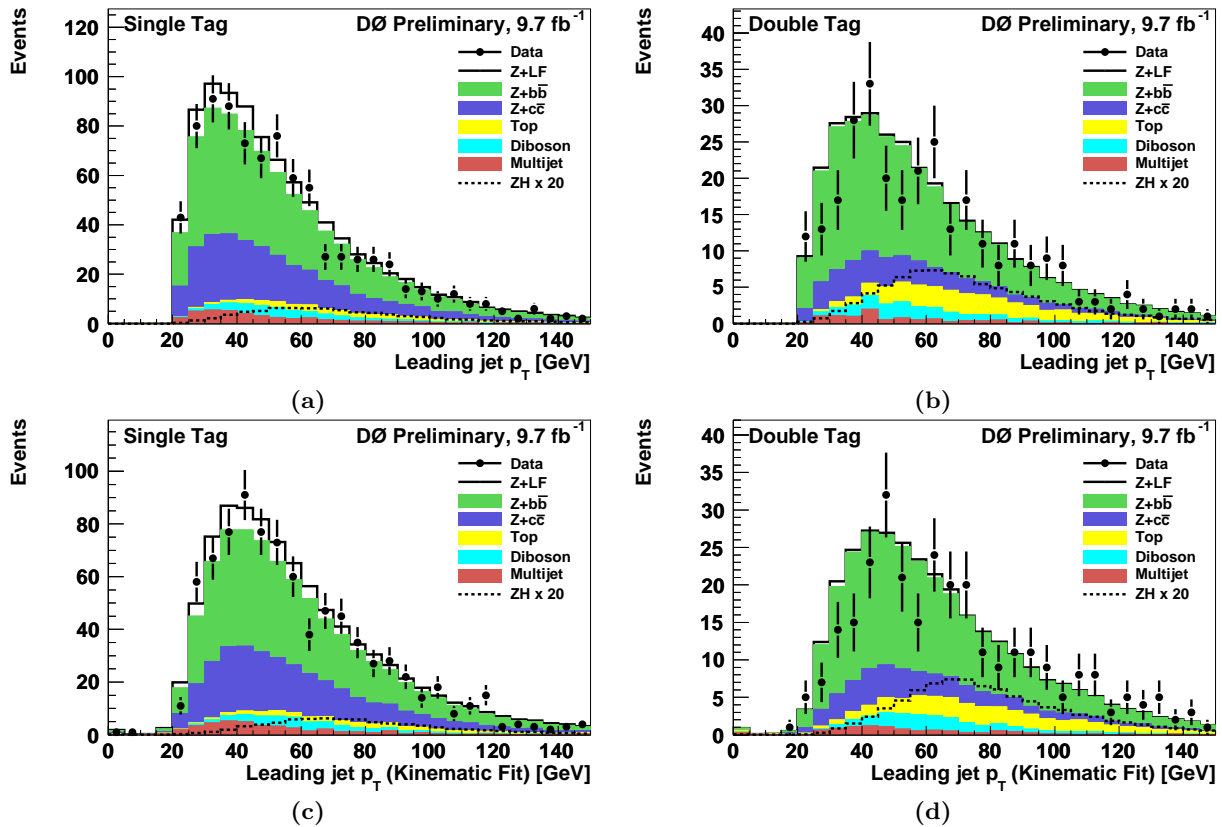


FIG. 4: Leading jet p_T distributions before the kinematic fit in (a) ST events, and (b) DT events; and after the kinematic fit in (c) ST events and (d) DT events, combined for all lepton channels. Signal distributions are shown with the SM cross section multiplied by 20.

reduces the impact of many of the remaining systematic uncertainties on the background size (except those related to b -tagging), but changes to the shape of the RF output distribution persist and are accounted for. Additional sources of systematic uncertainty include: jet energy scale, jet energy resolution, jet identification efficiency, b -tagging and trigger efficiencies, PDF uncertainties [29], data-determined corrections to the model for Z +jets, and modeling of the underlying event. The uncertainties from the factorization and renormalization scales in the simulation of Z +jets are estimated by scaling these parameters by factors of 0.5 and 2.

VII. HIGGS SEARCH RESULTS

We use the RF output distributions for the ST and the DT samples in each channel and the corresponding systematic uncertainties to set limits. To take advantage of the sensitivity in the more discriminating channels, we provide separate distributions for each channel to the limit-setting program.

Since no excess is observed, we proceed to set 95% C.L. limits on the ZH cross section with a modified frequentist (CLs) method that uses the log likelihood ratio (LLR) of the signal+background hypothesis to the background-only hypothesis [30]. To minimize the effect of systematic uncertainties, the likelihoods of the B and S+B hypotheses are maximized by independent fits which vary nuisance parameters that model the systematic uncertainties [31]. The correlations among systematic uncertainties are maintained across channels, backgrounds and signal, as appropriate. The RF distribution after the background-only fit, combined for all channels, is shown in Fig. 8 for ST and DT events separately. Also shown is the post-fit background subtracted RF distributions. In Fig. 9 the post-fit background subtracted RF distribution is shown for ST and DT events combined.

Fig. 10 shows the observed LLR as a function of Higgs boson mass. Also shown are the expected (median) LLRs for the background-only and signal+background hypotheses, together with the one and two standard deviation bands about the background-only expectation. A signal-like excess would result in a negative excursion in the observed LLR. The upper limits on the cross section, expressed as a ratio to the SM cross section, as a function of M_H are

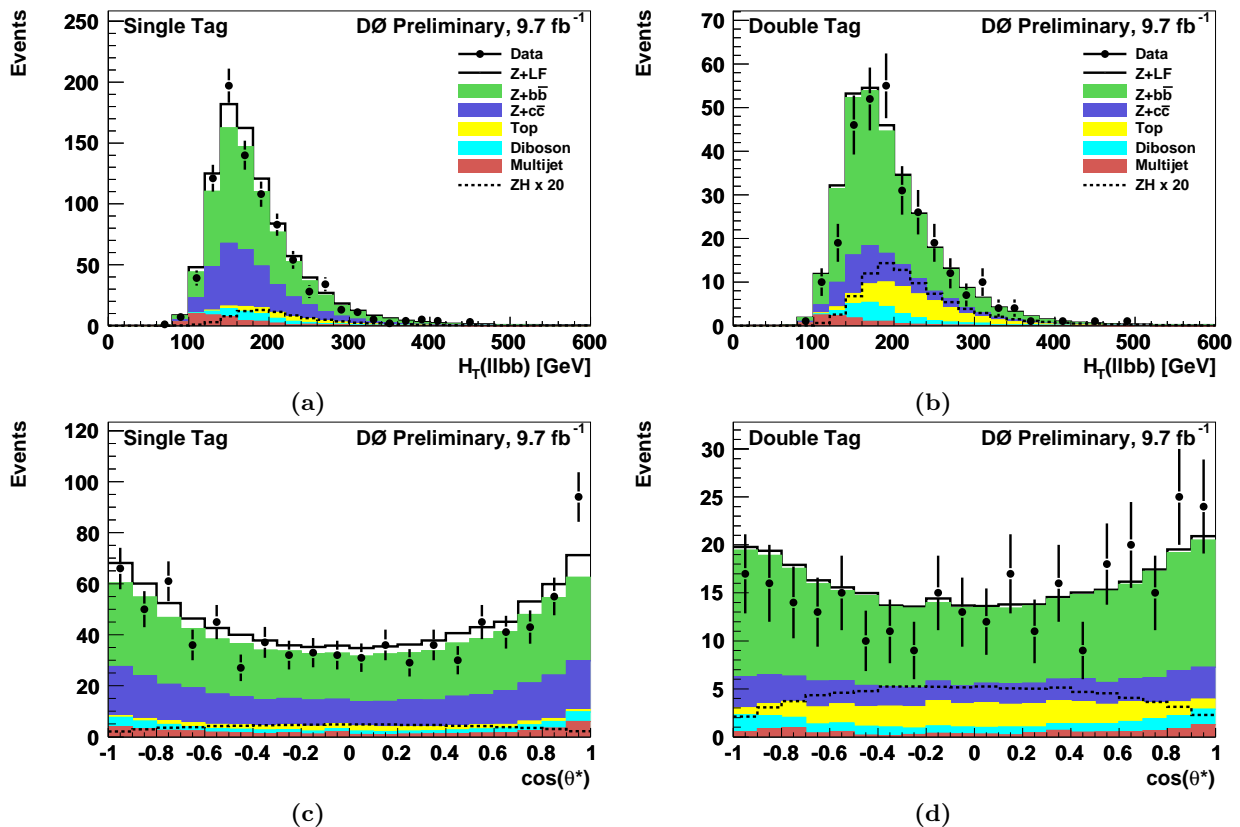


FIG. 5: $H_T(llbb)$ distributions in (a) ST events, and (b) DT events, and $\cos\theta^*$ distributions in (c) ST events, and (d) DT events, combined for all lepton channels. Signal distributions are shown with the SM cross section multiplied by 20.

presented in Table IV and Fig. 11. At $M_H = 115$ GeV, the observed (expected) limit on this ratio is 3.7 (4.2).

M_H (GeV)	100	105	110	115	120	125	130	135	140	145	150
Expected	3.2	3.5	3.8	4.2	5.0	5.9	7.7	10	14	21	34
Observed	2.2	2.4	2.8	3.7	5.1	6.9	11	15	20	30	49

TABLE IV: The expected and observed 95% C.L. upper limits on the SM Higgs boson production cross section for $ZH \rightarrow \ell^+\ell^-b\bar{b}$, expressed as a ratio to the SM cross section.

VIII. SUMMARY

In summary, we have searched for SM Higgs production in association with a Z boson in the final state of two charged leptons (electron or muon) and two b -quark jets using a 9.7 fb^{-1} data set. We set upper limits on the Higgs production cross section. The observed (expected) limit for $M_H = 115$ GeV is a factor of 3.7 (4.2) larger than the SM prediction.

Acknowledgments

We thank the staffs at Fermilab and collaborating institutions, and acknowledge support from the DOE and NSF (USA); CEA and CNRS/IN2P3 (France); FASI, Rosatom and RFBR (Russia); CNPq, FAPERJ, FAPESP and FUNDUNESP (Brazil); DAE and DST (India); Colciencias (Colombia); CONACyT (Mexico); KRF and KOSEF

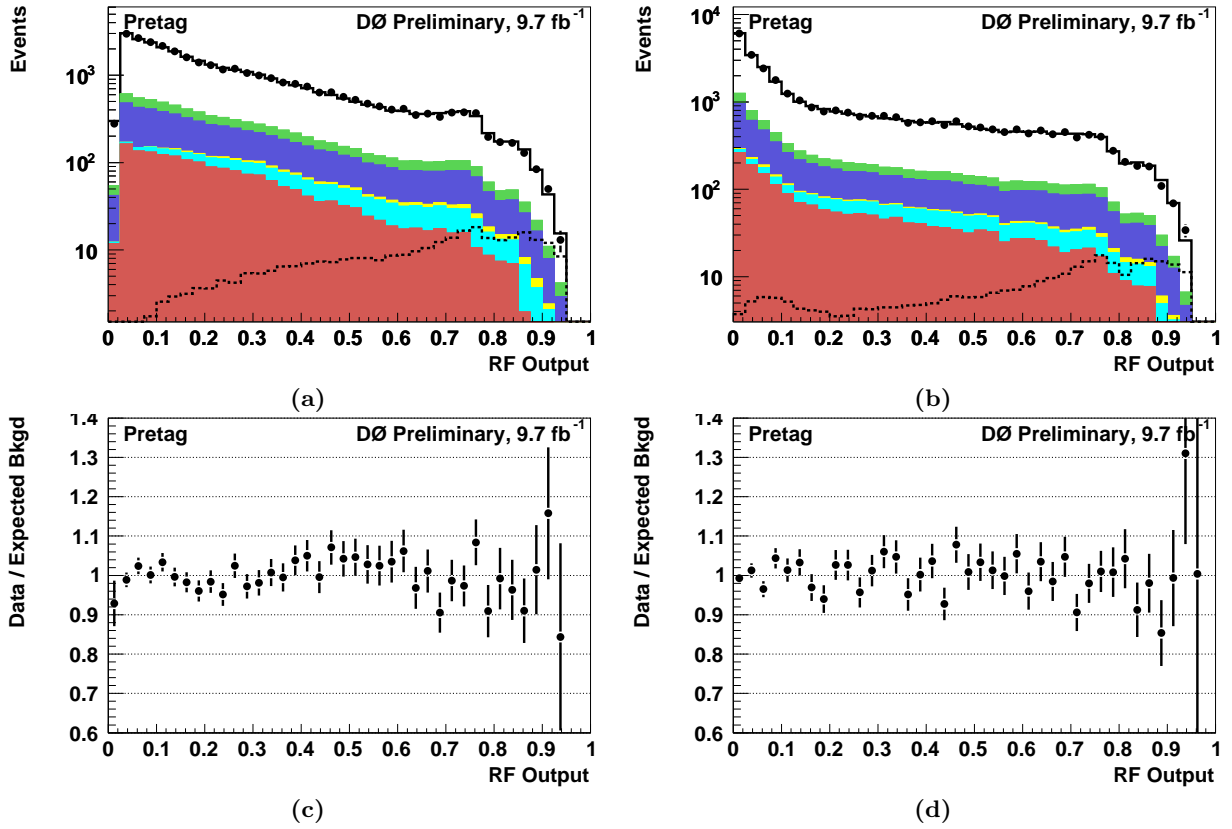


FIG. 6: Global RF output distributions for the ee , ee_{ICR} , $\mu\mu$ and $\mu\mu_{trk}$ channels combined assuming $M_H = 115$ GeV for (a) pretag events evaluated with the ST-trained RF and (b) pretag events evaluated with the DT-trained RF. Ratios of data to expected from (a) and (b) are shown in (c) and (d), respectively. Signal distributions are shown with the SM cross section multiplied by 20.

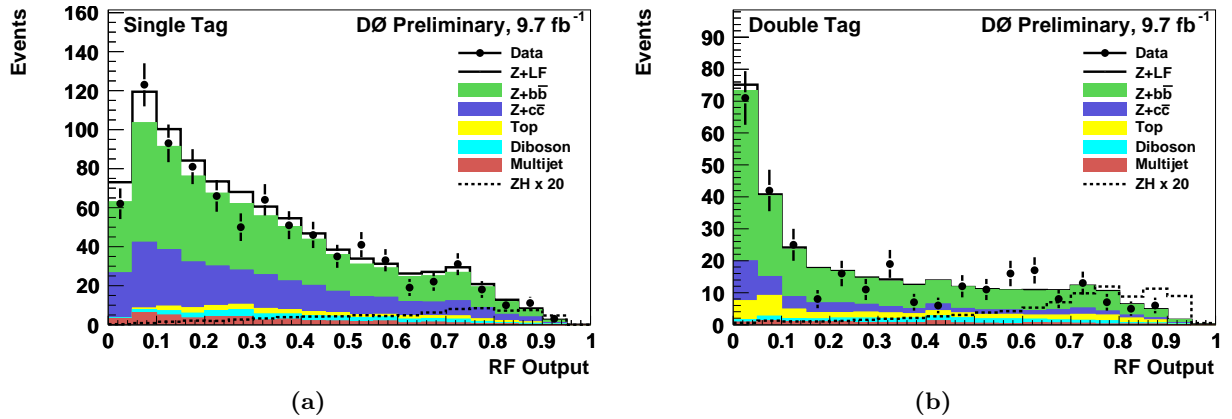


FIG. 7: RF output distributions for the ee , ee_{ICR} , $\mu\mu$ and $\mu\mu_{trk}$ channels combined assuming $M_H = 115$ GeV for (a) ST events evaluated with the ST-trained RF and (b) DT events evaluated with the DT-trained RF.

(Korea); CONICET and UBACyT (Argentina); FOM (The Netherlands); STFC and the Royal Society (United Kingdom); MSMT and GACR (Czech Republic); CRC Program and NSERC (Canada); BMBF and DFG (Germany);

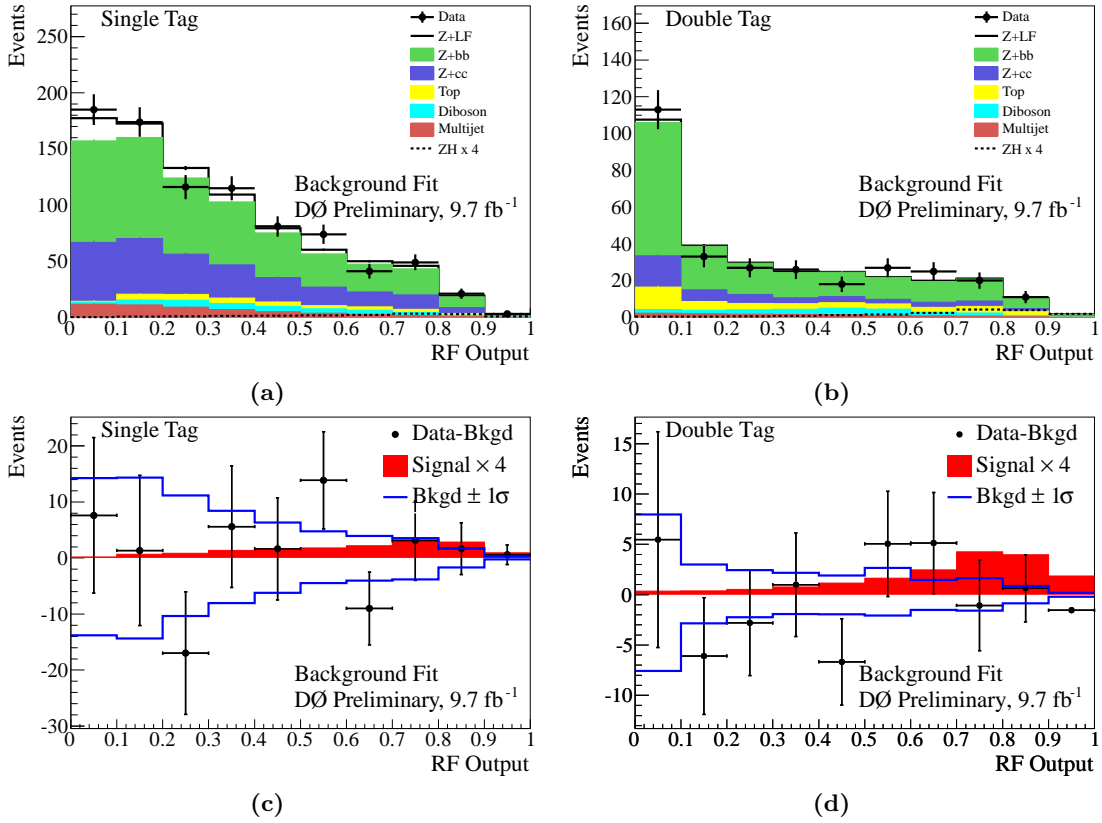


FIG. 8: RF output distributions for the ee , ee_{ICR} , $\mu\mu$ and $\mu\mu_{\text{trk}}$ channels combined assuming $M_H = 115$ GeV after the fit to the background-only model for (a) ST events evaluated with the ST-trained RF and (b) DT events evaluated with the DT-trained RF. Background-subtracted distributions for (a) and (b) are shown in (c) and (d), respectively. Signal distributions are shown with the SM cross section scaled to $4 \times$ SM prediction in (c) and (d).

SFI (Ireland); The Swedish Research Council (Sweden); and CAS and CNSF (China).

-
- [1] ALEPH, DELPHI, L3, and OPAL Collaborations, The LEP Working Group for Higgs Boson Searches, *Phys. Lett. B* **565**, 61 (2003).
- [2] LEP Electroweak Working Group
<http://lepewwg.web.cern.ch/LEPEWWG/>
- [3] Tevatron New Phenomena and Higgs Working Group
http://tevnphwg.fnal.gov/results/SM_Higgs_Summer_11/
- [4] CMS Collaboration, arXiv:1202.1488, (2012).
- [5] ATLAS Collaboration, arXiv:1202.1408v1, (2012).
- [6] V.M. Abazov *et al.* (D0 Collaboration), DØ Note 6299-CONF (2012)
 V.M. Abazov *et al.* (D0 Collaboration), DØ Note 6223-CONF (2011)
 V.M. Abazov *et al.* (D0 Collaboration), *Phys. Rev. Lett.* **104**, 071801 (2010).
- [7] V. M. Abazov *et al.* (D0 Collaboration), *Nucl. Instrum. Methods Phys. Res. Sect. A* **565**, 463 (2006);
 M. Abolins. *et al.*, *Nucl. Instrum. Methods Phys. Res. Sect. A* **584**, 75 (2008); R. Angstadt *et al.*, *Nucl. Instrum. Methods Phys. Res. Sect. A* **622**, 298 (2010)
- [8] V.M. Abazov *et al.* (D0 Collaboration), DØ Note 6166-CONF (2011).
- [9] V.M. Abazov *et al.* (D0 Collaboration), *Phys. Rev. Lett.* **105**, 251801 (2010).
- [10] V.M. Abazov *et al.* (D0 Collaboration), DØ Note 6080-CONF (2010).
- [11] V.M. Abazov *et al.* (D0 Collaboration), DØ Note 6256-CONF (2011).
- [12] Pseudorapidity is defined as $\eta = -\ln[\tan(\theta/2)]$, where θ is the polar angle relative to the proton beam direction. ϕ is defined to be the azimuthal angle in the plane transverse to the proton beam direction.
- [13] G. C. Blazey *et al.*, arXiv:hep-ex/0005012.

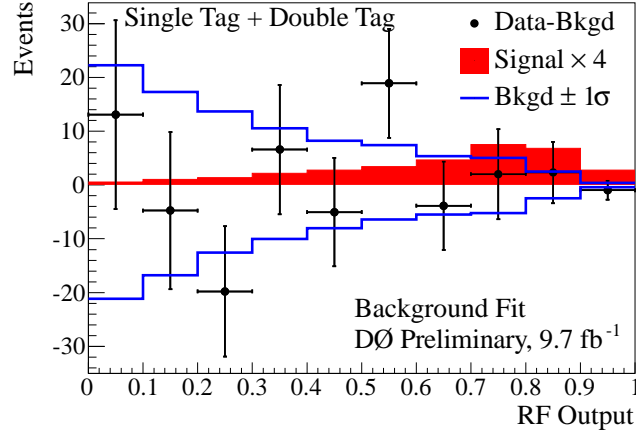


FIG. 9: Background subtracted RF distribution for $M_H=115$ GeV. Both ST and DT events are included. The blue lines indicate the uncertainty after the fit to the SM background model. The solid red distributions indicates the signal, scaled to $4 \times$ SM prediction.

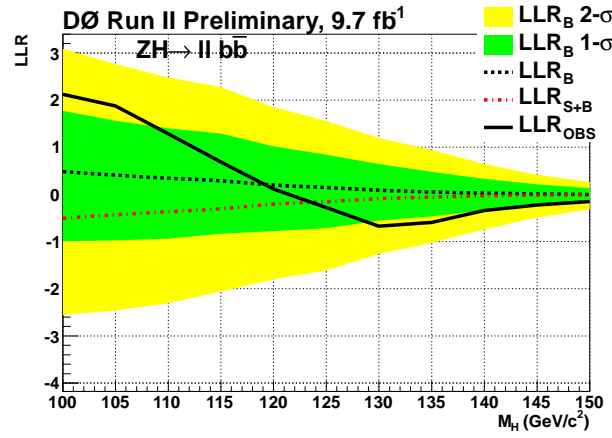


FIG. 10: Observed LLR as a function of Higgs boson mass. Also shown are the expected LLRs for the background-only (B) and signal+background (S+B) hypotheses, together with the one and two σ bands about the background-only expectation.

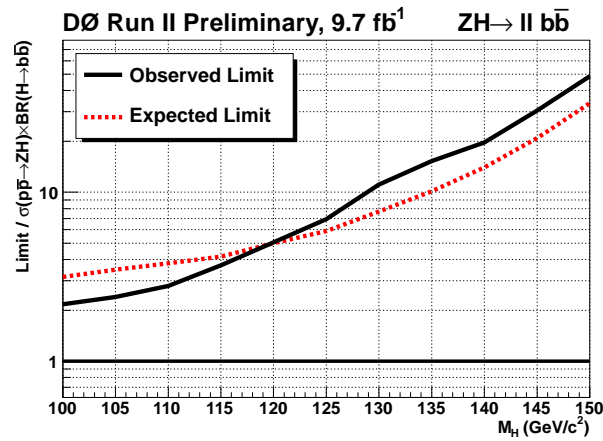


FIG. 11: Expected and observed 95% C.L. cross section upper limits, expressed as a ratio to the SM cross section.

- [14] V. M. Abazov *et al.* (D0 Collaboration), Nucl. Instrum. Methods in Phys. Res. Sect. A **620**, 490 (2010).
- [15] T. Sjöstrand *et al.*, Comput. Phys. Commun. **135**, 238 (2001). Version 6.409 was used.
- [16] M. L. Mangano *et al.*, J. High Energy Phys. **0307**, 001 (2003). Version 2.11 was used.
- [17] J. Pumplin *et al.*, J. High Energy Phys. **07**, 012 (2002).
- [18] R. Brun, F. Carminati, CERN Program Library Long Writeup W5013 (1993).
- [19] J. Baglio and A. Djouadi, arXiv:1003.4266v2 [hep-ph].
- [20] S. Dittmaier *et al.* [LHC Higgs Cross Section Working Group], arXiv:1101.0593v2 (2011).
- [21] J. Campbell and R.K. Ellis, <http://mcfm.fnal.gov/>.
- [22] U. Langefeld, S. Moch, and P. Uwer, Phys. Rev. D **80**, 054009 (2009).
- [23] R. Hamberg, W.L. van Neerven and W.B. Kilgore, Nucl. Phys. B**359**, 343 (1991), [*Erratum ibid.* B **644**, 403 (2002)].
- [24] V. M. Abazov *et al.* (D0 Collaboration), Phys. Rev. Lett. **100**, 102002 (2008).
- [25] T. Gleisberg *et al.*, J. High Energy Phys. 02 (2004) 056; J. Alwall *et al.*, Eur. Phys. J. C **53**, 473 (2008).
- [26] C. Balazs and C.-P. Yuan. Phys.Rev.D56:5558-5583,1997.
- [27] S. Parke and S. Veseli, Phys. Rev. D **60**, 093003 (1999).
- [28] A. Hoecker *et al.*, arXiv:physics/0703039v5 [physics.data-an].
- [29] D. Stump *et al.*, J. High Energy Phys. **10**, 046 (2003).
- [30] T. Junk, Nucl. Instrum. Methods Phys. Res., Sect. A **434**, 435 (1999); A. Read. J. Phys. G **28** 2693 (2002).
- [31] W. Fisher, FERMILAB-TM-2386-E (2007).